J. Fluid Mech. (1983), *vol.* 135 *pp.* 1–26
Printed in Great Britain

Three-dimensional tertiary motions in a plane shear layer

By M. NAGATA AND F. H. BUSSE
Department of Earth and Space Sciences, University of California at Los Angeles

(Received 22 November 1982 and in revised form 4 May 1983)

The nonlinear evolution of instabilities of a plane-parallel shear flow with an inflection-point profile is studied. The particular example of the cubic-profile flow generated in an inclined layer heated from above and cooled from below is chosen because it exhibits supercritical bifurcations for secondary and tertiary flows. Since the limit of small Prandtl number is assumed, buoyancy effects caused by temperature perturbations are negligible. The analysis describes first the transition to transverse roll-like vortices which become unstable at slightly supercritical Grashof numbers to a vortex-pairing instability with alternating pairing in the spanwise direction. Three-dimensional finite-amplitude solutions for this tertiary mode of motion are computed and discussed. Finally the question of the stability of the tertiary flow is addressed.

1. Introduction

Theoretical and experimental studies in recent years of subsequent instabilities in thermal convection and in circular Couette flow have led to a deeper understanding of the transition from laminar to turbulent fluid flow. For reviews of the sequences of bifurcations found in convection and in circular Couette flow see the articles by Busse (1981) and DiPrima & Swinney (1981). It is generally believed that similar sequences of bifurcations exist in problems of plane-parallel shear flow. But those bifurcations are usually not observable because they occur mostly subcritically. The most effective mechanism of shear-flow instability is prevented by the absence of an inflection point in the profile in typical cases of plane parallel flows such as Poiseuille or Hagen–Poiseuille flow. The resulting delay of the onset of instability by infinitesimal disturbances is the main reason for the subcritical finite-amplitude instability and the direct transition into a turbulent state of motion found in those cases. Numerical simulations (Orzag & Patera 1980; Orszag & Kells 1980) and stability studies of Tollmien–Schlichting waves (Herbert 1981*a*, 1983) have provided some insights into the mechanism of transition to turbulence to Poiseuille and plane Couette flow. For a review of recent theoretical and experimental work on the transition to turbulence in channel flow see Herbert (1981*b*). The complexity of instability of shear flows without inflection point, however, makes it difficult to get a comprehensive picture of the manifolds of solutions involved in the various bifurcations. For this reason a study of the series of bifurcations starting with the inertial instability of a shear flow with an inflection point is likely to shed some new light on the general problem of transition to turbulence in plane parallel shear flow. Moreover, the possibility of supercritical bifurcations offers new opportunities for comparison with experimental observations. This point of view has motivated the investigation presented in this paper.

Although the inertial mechanism of instability of plane parallel shear flow has been analyzed extensively since the early work of Helmholtz (1868) and Kelvin (1871) there have been few opportunities for quantitative comparisons with laboratory measurements. According to Rayleigh (1880) the inertial instability requires a point of inflection in the profile; but there are few plane-parallel flows with an inflection point which can be realized in the laboratory even in an approximate sense. The lack of observational evidence has inhibited to some extent the study of the post-instability problem. Benney & Bergeron (1969) have derived nonlinear inviscid solutions for the transverse 'cat's-eye'-like eddies that arise from the instability and later workers have taken into account the effects of viscosity (Haberman 1972; Huerre 1980; Huerre & Scott 1980). A weakly nonlinear analysis of growing two-dimensional disturbances has been given by Schade (1964) for the hyperbolic tangent profile which is the exemplary case of an inflexion-point profile. The stability with respect to two-dimensional disturbances of the periodic flow studied by Schade was investigated by Kelly (1967), who found growing disturbances with twice the wavelength of the secondary flow. Perhaps closest in its goals to the present analysis is the work by Pierrehumbert & Widnall (1982) who studied the stability with respect to three-dimensional disturbances of a family of coherent shear-layer vortices described by a solution of the inviscid equations of motion found by Stuart (1967). Like most of the work mentioned above Pierrehumbert & Widnall (1982) neglect effects of viscosity even though the Reynolds numbers at which the transitions to two-dimensional and to three-dimensional motions must be expected are not very large. Aside from the effects of viscosity, the comparison with experimental observations is complicated by the choice of mathematically convenient but physically not realizable basic shear-flow profiles in the theoretical work. It thus seems of special interest to investigate secondary and tertiary flows arising from the instability of a basic flow that is an actual solution of the Navier–Stokes equation of motion for reasonable forces.

The plane-parallel flow on which the analysis of this paper is focused has a profile described by a cubic polynomial. It is realized when an infinitely extended fluid layer is bounded by two rigid planes that are kept at constant but different temperatures. The flow vanishes only in the exceptional case when the layer is horizontal with respect to gravity. To avoid any confusion with the problem of convective instability, we shall refer to the case of an inclined layer heated on the upper side even though buoyancy-driven instabilities do not occur in the limit in which the problem will be considered. The limit of vanishing Prandtl number P is not easily realizable in experiments because only liquid metals possess values of P that are small compared to unity. But results of linear stability theory indicate that hydrodynamic effects dominate over thermal effects even for $P = 1$, at least in the case of a vertical layer (Vest & Arpaci 1969). Thus reasonable agreement between theoretical predictions and experimental observations can be expected in the case of a vertical layer of air heated from one side and cooled from the other. As far as two-dimensional aspects of the problem are concerned, such a comparison is indeed possible, as will be pointed out later in this paper. But observations of three-dimensional structures are not available at this time.

2. Mathematical formulation of the problem

We consider a layer of a Boussinesq fluid inclined with the angle χ with respect to the horizontal plane. The temperatures T_2 and T_1 with $T_2 > T_1$ are prescribed on the upper and lower boundaries of the layer. An angle χ equal to or less than $\frac{1}{2}\pi$ will

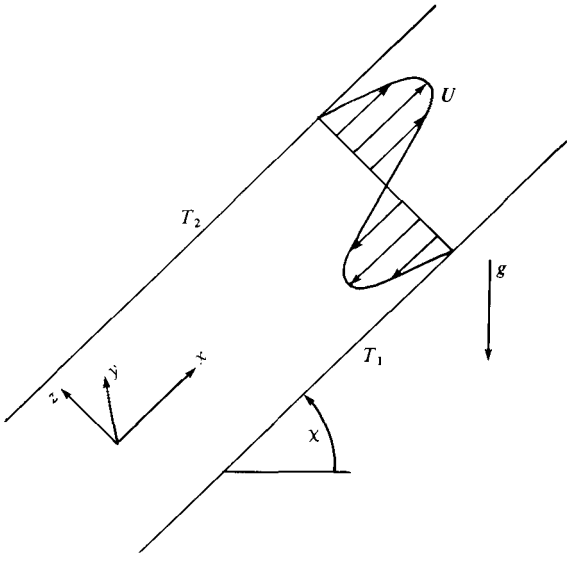

FIGURE 1. Geometrical configuration of the inclined fluid layer heated from above and exhibiting a plane-parallel shear flow with cubic profile as basic solution.

be assumed in general. For angles $\chi > \frac{1}{2}\pi$, T_1 is prescribed at the upper and T_2 is prescribed at the lower boundary. Although the present analysis for the limit of vanishing Prandtl number is valid for this case as well, a competing thermal instability occurs at higher Prandtl numbers. Using the thickness d of the layer, d^2/ν and $(T_2-T_1)/Gr\,P$ as scales for length, time and temperature respectively, we write the equations of motion for the velocity vector $\boldsymbol{u}$ and the heat equation for the deviation θ for the purely conductive state of the temperature distribution in dimensionless form:

$$\frac{\partial}{\partial t}\boldsymbol{u}+\boldsymbol{u}\cdot\boldsymbol{\nabla u} = -\boldsymbol{\nabla}\pi + Gr\sin\chi\boldsymbol{k}\cdot\boldsymbol{ri}+(\cos\chi\boldsymbol{k}+\sin\chi\boldsymbol{i})\,\theta+\nabla^2\boldsymbol{u}, \tag{2.1a}$$

$$\boldsymbol{\nabla}\cdot\boldsymbol{u} = 0, \tag{2.1b}$$

$$\frac{\partial}{\partial t}\theta+\boldsymbol{u}\cdot\boldsymbol{\nabla}\theta = -Gr\,\boldsymbol{u}\cdot\boldsymbol{k}+P^{-1}\nabla^2\theta. \tag{2.1c}$$

The Grashof number and Prandtl number are defined by

$$Gr \equiv \gamma g(T_2-T_1)\,d^3/\nu^2, \quad P = \nu/\kappa,$$

where ν, κ, γ and g denote viscosity, thermal diffusivity, coefficient of thermal expansion and acceleration due to gravity respectively. The unit vectors $\boldsymbol{k}$ and $\boldsymbol{i}$ point in the directions normal and parallel to the layer such that the direction of gravity is given by $-\cos\chi\boldsymbol{k}-\sin\chi\boldsymbol{i}$. Terms that can be written as gradients have been combined into the expression $\boldsymbol{\nabla}\pi$. As indicated in figure 1, we shall use a Cartesian system of coordinates with the origin on the median plane of the layer and with the z-and x-coordinates in the directions of $\boldsymbol{k}$ and $\boldsymbol{i}$ respectively. The basic solution of (2.1) exhibiting the same symmetry as the physical conditions of the problem is given by

$$\boldsymbol{u} = U\boldsymbol{i} \equiv \tfrac{1}{6}\boldsymbol{i}\,G(\tfrac{1}{4}z-z^3), \quad \theta \equiv 0, \tag{2.2}$$

where the definition $G \equiv Gr\sin\chi$ has been introduced. The analysis of this paper is

concerned with the properties of solutions bifurcating from the basic state (2.2). The boundary condition

$$\boldsymbol{u} = 0 \quad (z = \pm\tfrac{1}{2}) \tag{2.3}$$

used in deriving (2.2) could eventually be replaced by the condition

$$\boldsymbol{u} = \pm U_0 \boldsymbol{i} \quad (z = \pm\tfrac{1}{2}), \tag{2.4}$$

giving rise to a manifold of solutions which can be analysed in the same way as the solutions satisfying (2.3) (Nagata 1983); but in this paper the attention will be focused on the special case $U_0 = 0$.

The stability of the basic solution (2.2) with respect to infinitesimal disturbances has been studied by a number of authors as a function of the Prandtl number. Rudakov (1967), Korpela, Gözüm & Baxi (1973) and Ruth (1979) considered a vertical layer, $\chi = \frac{1}{2}\pi$, and found that the critical Grashof number G_c changes by less than ten per cent in the regime $0 \leqslant P \leqslant 10$, while some change in the character of the solution occurs in the neighbourhood of $P = 1.75$. The instability is clearly hydrodynamic in origin, although thermal effects become noticeable for larger Prandtl numbers. In this paper we make use of the weak Prandtl-number dependence by assuming the limit of vanishing Prandtl number. In this limit thermal conduction is so effective in comparison with heat advection that the deviation θ from the state of pure conduction vanishes even for general three-dimensional motions.

It is convenient to separate the velocity field $\boldsymbol{u}$ into an average part $\hat{U}\boldsymbol{i}$ and a fluctuating part $\check{\boldsymbol{u}}$:

$$\boldsymbol{u} = \hat{U}\boldsymbol{i} + \check{\boldsymbol{u}}, \tag{2.5}$$

where $\hat{U}(z,t)\,\boldsymbol{i}$ is equal to the average of $\boldsymbol{u}$ over x- and y-coordinates. In principle there could be an average component in the y-direction as well, but since such a component has not been encountered in the analysis it is not mentioned explicitly in (2.5). For the fluctuating component we introduce the general representation of a solenoidal vector field

$$\check{\boldsymbol{u}} = \boldsymbol{\nabla} \times (\boldsymbol{\nabla} \times \boldsymbol{k}\phi) + \boldsymbol{\nabla} \times \boldsymbol{k}\psi \equiv \boldsymbol{\delta}\phi + \boldsymbol{\epsilon}\psi \tag{2.6}$$

which allows us to eliminate (2.1*b*) from the problem. By taking the z-components of the curl and the curl curl of (2.1*a*) the following equations are obtained:

$$\nabla^2 \Delta_2 \psi = \left(\hat{U}\frac{\partial}{\partial x} + \frac{\partial}{\partial t}\right)\Delta_2 \psi - \frac{\partial}{\partial z}\hat{U}\frac{\partial}{\partial y}\Delta_2 \phi + \boldsymbol{k}\cdot\boldsymbol{\nabla} \times [\check{\boldsymbol{u}}\cdot\boldsymbol{\nabla}\check{\boldsymbol{u}}], \tag{2.7a}$$

$$\nabla^4 \Delta_2 \phi = \left(\hat{U}\frac{\partial}{\partial x} + \frac{\partial}{\partial t}\right)\nabla^2 \Delta_2 \phi - \frac{\partial^2}{\partial z^2}\hat{U}\frac{\partial}{\partial x}\Delta_2 \phi + \boldsymbol{k}\cdot\boldsymbol{\nabla} \times (\boldsymbol{\nabla} \times [\check{\boldsymbol{u}}\cdot\boldsymbol{\nabla}\check{\boldsymbol{u}}]), \tag{2.7b}$$

where $\Delta_2 = \partial^2/\partial x^2 + \partial^2/\partial y^2$ is the two-dimensional Laplacian.

The mean flow $\hat{U}$ is given by

$$\hat{U} \equiv U + \check{U},$$

where $\check{U}$ satisfies the equation

$$\left(\frac{\partial}{\partial t} - \frac{\partial^2}{\partial z^2}\right)\check{U} = \frac{\partial}{\partial z}\overline{\left(\frac{\partial^2}{\partial x\,\partial z}\phi + \frac{\partial}{\partial y}\psi\right)\Delta_2 \phi}. \tag{2.8}$$

The bar indicates the average over the x- and y-coordinates. If a non-vanishing Reynolds stress in the y-direction did exist,

$$\overline{\left(\frac{\partial^2}{\partial y\,\partial z}\phi - \frac{\partial}{\partial x}\psi\right)\Delta_2 \phi} \not\equiv 0, \tag{2.9}$$

then a component of the mean flow in the y-direction would be obtained. But in all cases investigated in the present work (2.9) was never satisfied.

When (2.7) are linearized with respect to ϕ and ψ, Squire's (1933) theorem is applicable. Accordingly, the instability of the cubic profile flow (2.2) assumes the form of y-independent transverse vortices with vanishing function ψ. Since the inflection point coincides with the zero of the mean-flow profile (2.2) the phase velocity of the strongest growing vortices vanishes. Because of the symmetry of the problem the vortices remain steady with respect to the chosen frame of reference as they equilibrate at finite amplitude. The analysis thus starts with the derivation of two-dimensional steady finite-amplitude solutions of (2.7), (2.8) in §3. The stability of these solutions with respect to arbitrary infinitesimal disturbances is investigated in §4. Examples of three-dimensional finite-amplitude flow arising from those disturbances are computed in §5. Finally a stability analysis of the three-dimensional steady flow is given in §6. Thus the evolution from laminar to turbulent flow will have been followed up to the third bifurcation.

3. Steady transverse vortices

Finite-amplitude steady two-dimensional solutions of (2.7) and (2.8) can be obtained by representing ϕ and $\check{U}$ in terms of orthogonal functions satisfying the boundary conditions:

$$\phi = \sum_{m=-\infty}^{\infty} \sum_{l=1}^{\infty} a_{lm} f_l(z) \exp\{im\alpha x\}, \tag{3.1a}$$

$$\check{U} = \sum_{n=1}^{\infty} C_n \sin 2n\pi z, \tag{3.1b}$$

where the functions $f_l(z)$ introduced by Chandrasekhar (1961) are defined by

$$f_l(z) = \begin{cases} \dfrac{\sinh \mu_{\frac{1}{2}l} z}{\sinh \frac{1}{2}\mu_{\frac{1}{2}l}} - \dfrac{\sin \mu_{\frac{1}{2}l} z}{\sin \frac{1}{2}\mu_{\frac{1}{2}l}} & (l \text{ even}), \\ \dfrac{\cosh \nu_{\frac{1}{2}(l+1)} z}{\cosh \frac{1}{2}\nu_{\frac{1}{2}(l+1)}} - \dfrac{\cosh \nu_{\frac{1}{2}(l+1)} z}{\cosh \frac{1}{2}\nu_{\frac{1}{2}(l+1)}} & (l \text{ odd}). \end{cases} \tag{3.2}$$

The numbers μ_i and ν_i are defined as the positive roots of the equations

$$\left.\begin{aligned} \coth \tfrac{1}{2}\mu_i - \cot \tfrac{1}{2}\mu_i &= 0, \\ \tanh \tfrac{1}{2}\nu_i - \tan \tfrac{1}{2}\nu_i &= 0 \end{aligned}\right\} \quad (i = 1, 2, \ldots). \tag{3.3}$$

According to (3.2) the function $f_l(z)$ and its first derivative vanish at the boundaries $z = \pm\frac{1}{2}$, which ensures that both components of $\boldsymbol{u}$ vanish there.

Because only x-derivatives of ϕ enter the basic equations, $m = 0$ can be excluded in the representation (3.1a) of ϕ. Since ϕ is a real function, the complex coefficient must satisfy

$$a_{l,-m} = a_{lm}^*, \tag{3.4}$$

where the asterisk denotes the complex conjugate. The symmetry of the problem permits the imposition of an additional constraint

$$a_{lm} = \begin{cases} a_{lm}^* & (l+m \text{ even}), \\ -a_{lm}^* & (l+m \text{ odd}). \end{cases} \tag{3.5}$$

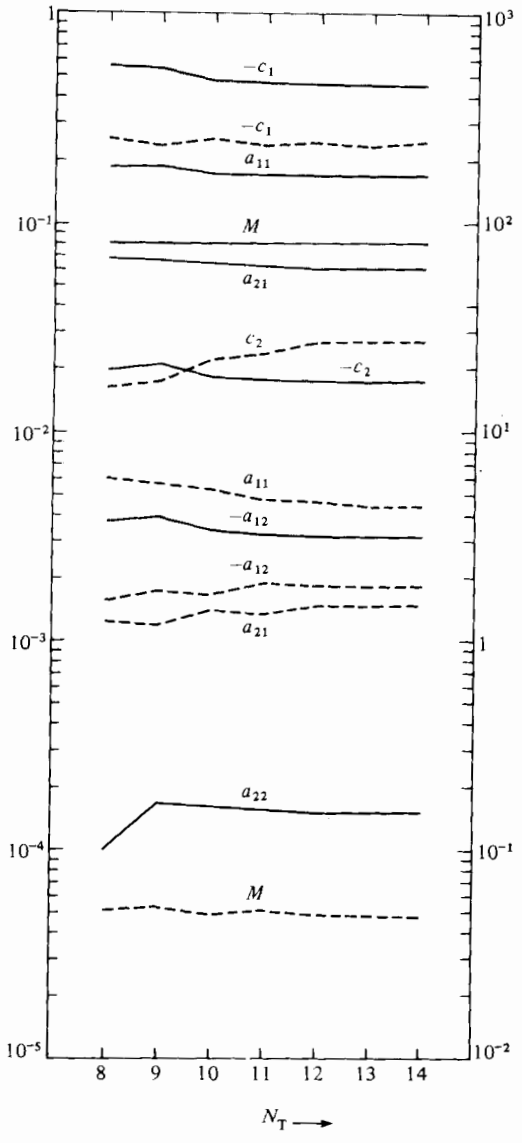

FIGURE 2. Convergence of coefficients a_{nm} and c_n as functions of the truncation parameter N_1 for the Grashof numbers $G = 8050$ (solid lines, left ordinate) and $G = 50000$ (dashed lines, right ordinate). The truncation parameter N_2 for the coefficients C_n is given by $N_2 = N_1 + 3$. The wavenumber $\alpha = 2.6$ was used.

This symmetry would be destroyed if the mean-flow profile was no longer antisymmetric with respect to $z = 0$, as for example in the case of a superimposed Poiseuille flow.

By multiplying (2.7) by $f_\lambda(z)\exp\{-i\mu\alpha x\}$ and (2.8) by $\sin 2\nu\pi z$ and averaging the result over the fluid layer, nonlinear algebraic equations for the coefficients a_{lm}, C_n are obtained. As the parameters λ, μ, ν run through all admissible integer values, an infinite system of equations results which must be truncated in order to permit a numerical solution. Guided by the experience in related problems of convection (Busse

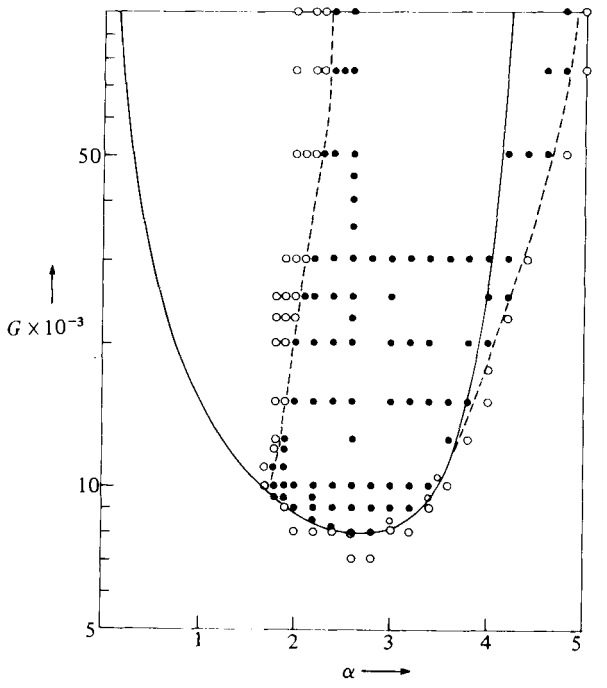

FIGURE 3. The Grashof number G as a function of the wavenumber α according to linear theory (solid line). Dots indicate parameter values for which nonlinear two-dimensional solution have been obtained. Open circles indicate points when attempts to obtain a nonlinear solution failed.

1967; Clever & Busse 1974), we shall neglect all coefficients and all equations with subscripts satisfying the conditions

$$l+|m| > N_1, \quad n > N_2. \tag{3.6a, b}$$

The resulting finite system of equations is solved by a Newton–Raphson iteration method. The truncation parameters N_1 and N_2 are then each increased by 2 and the new solution is compared with the old one. If the coefficients with low subscripts change very little and if mean quantities such as the momentum transport by the vortices change by less than a few percent, the numerical approximation is regarded as satisfactory. The choice $N_1 = 11$, $N_2 = 8$ was used in most calculations. $N_2 = 6$ would be consistent with $N_1 = 11$; but, since an increase in N_2 is not as costly as an increase of N_1 in terms of computational expenses, a somewhat larger value of N_2 has been used.

To test the rate of convergence of solutions with increasing N_1, the truncation parameter has been increased to a value as high as $N_1 = 14$ for some solutions. Figure 2 shows that typical coefficients exhibit little change for $N_1 \geqslant 11$. This appears to be true even for values of G as high as $G = 5 \times 10^4$, although $N_1 = 12$ provides a noticeable improvement over $N_1 = 11$. But, since most of the analysis is focused on properties of the solutions at lower values of G, the truncation $N_1 = 11$ appears to be sufficiently accurate.

Steady solutions have been obtained for numerous values of G exceeding the critical value of $G_c = 7930.0$ determined by linear theory as shown in figure 3. No subcritical finite-amplitude solution was found. But for values of α beyond the critical value $\alpha_c = 2.69$, steady solutions exist outside the region bounded by the function $G(\alpha)$

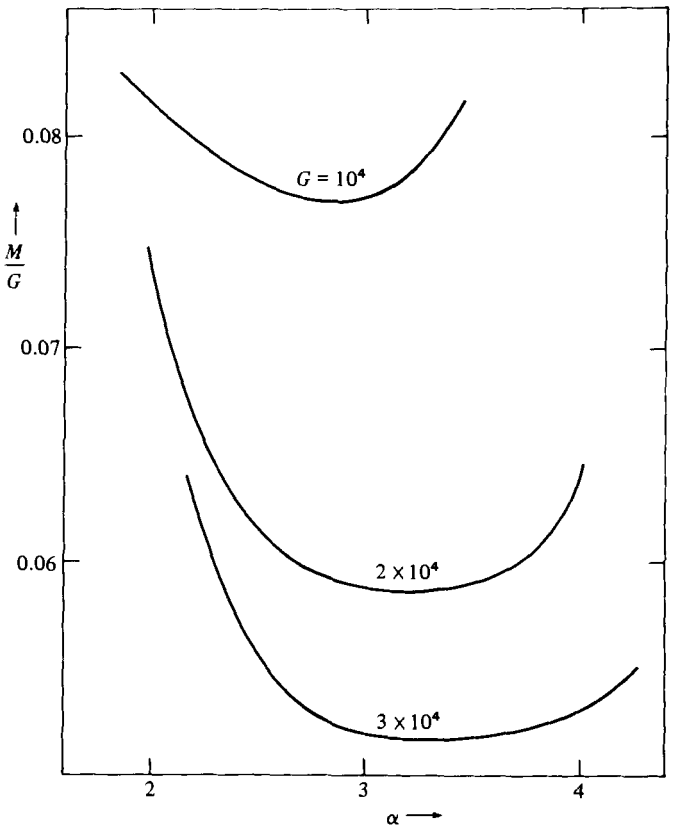

FIGURE 4. The momentum transport M as a function of the wavenumber α for three different Grashof numbers G.

deduced from linear theory, the function $G(\alpha)$ increases rather steeply such that it becomes difficult to determine it for $\alpha \gtrsim 5$. The boundary of the region of nonlinear solutions increases more gradually with α. The nonlinear nature of this boundary can be seen in the momentum transport plotted in figure 4 and discussed below.

For $\alpha \lesssim 1.8$ a steady solution could not be obtained. The numerical method produced instead the solution with 2α as basic wavenumber. It is evident from figure 3 that the wavenumber below which steady solutions could not be obtained corresponds to one half of the wavenumber at the boundary of the region of steady solution on the right. A similar phenomenon has been observed in computations of convection rolls (Clever & Busse 1974). Because of an additional symmetry property in the latter problem, solutions could not be obtained if 3α (instead of 2α) was within the domain bounded by the curve derived from linear theory. Because the Eckhaus instability always precedes the numerical instability, the steady solutions affected by the latter are not of much interest.

A measure of the strength of the transverse vortices can be obtained from the change of the stress exerted on the boundaries. Integration of equation (2.8) yields in the steady case

$$\frac{\mathrm{d}}{\mathrm{d}z}\check{U} = -\overline{\Delta_2 \phi \frac{\partial^2 \phi}{\partial x\, \partial z}} + \left\langle \Delta_2 \phi \frac{\partial^2 \phi}{\partial x\, \partial z} \right\rangle, \tag{3.7}$$

where the angle brackets indicate the average over the entire fluid layer. The last term in (3.7) is the constant of integration, which has been determined such that $\check{U}$

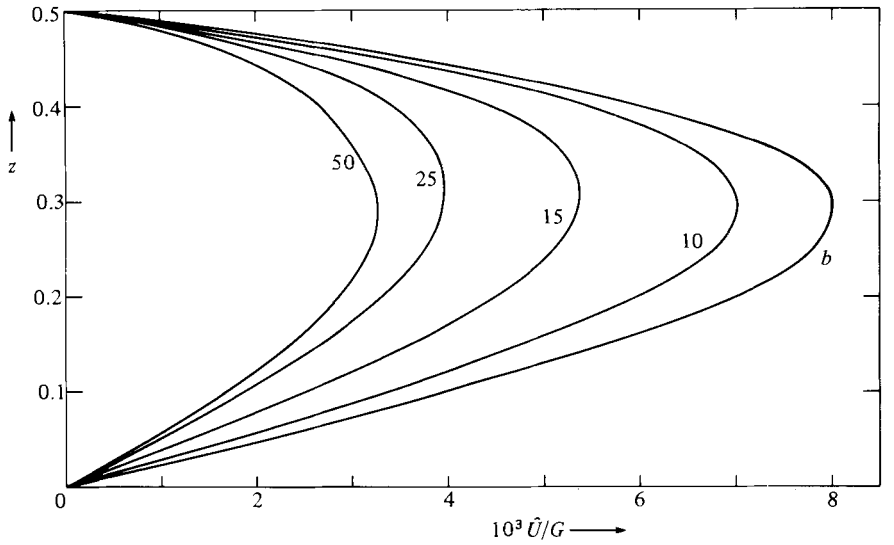

FIGURE 5. The mean flow $\hat{U}$ as a function of z for different Grashof numbers $G \times 10^{-3}$. The wavenumber α of transverse vortices is fixed at 2.6. The profile $\hat{U}$ is antisymmetric with respect to $z = 0$. The undisturbed flow $\hat{U} = U$ is indicated by b.

vanishes at the boundaries. This constant enters the expression for the dimensionless momentum transport at $z = \pm\frac{1}{2}$

$$M = \tfrac{1}{12}G - \left\langle \Delta_2 \phi \frac{\partial^2 \phi}{\partial x\, \partial z} \right\rangle. \tag{3.8}$$

The expression (3.8) has been plotted as a function of α for various values of G in figure 4. The transverse vortices strongly reduce the stress exerted on the boundaries. Vortices with wavenumbers α outside the central range are not as effective in transporting momentum, but they retain a finite amplitude as α approaches the largest value for which solutions could be obtained for $G = 2 \times 10^4$ and $G = 3 \times 10^4$. This property proves the finite-amplitude character of solutions at the dashed boundary of figure 3.

Since the transverse vortices tend to homogenize the mean momentum in the interior of the layer, the mean vorticity is reduced. Figure 5 shows that the profile of the mean flow retains approximately its cubic shape. A saturation effect is noticeable in so far as there is relatively little change between the curves for $G = 2.5 \times 10^4$ and $G = 5 \times 10^4$. As must be expected from our above discussion, the reduction of the mean flow is largest for vortices with wavenumbers in the central regime around $\alpha = 3.0$ as shown in figure 6.

In order to visualize the transverse vortices, both the disturbance stream function $\partial\phi/\partial x$ and the stream function of the total flow have been plotted in figure 7. The inclination of the boundary between the rolls shown in the upper part of the figure indicate the momentum transport in the direction opposite to the viscous stress of the cubic profile in the median plane of the layer. In the lower part of the figure the familiar 'cat's-eye' pattern is exhibited. This streamline picture resembles closely the observed one in the experiments of Vest & Arpaci (1969). While the gross properties of the two-dimensional steady flow remain approximately valid after three-dimensional steady disturbances develop, the streamline pattern and other details of the flow will be changed. Before proceeding to the discussion of three-dimensional steady flows, we describe the stability properties of the transverse-vortex flow.

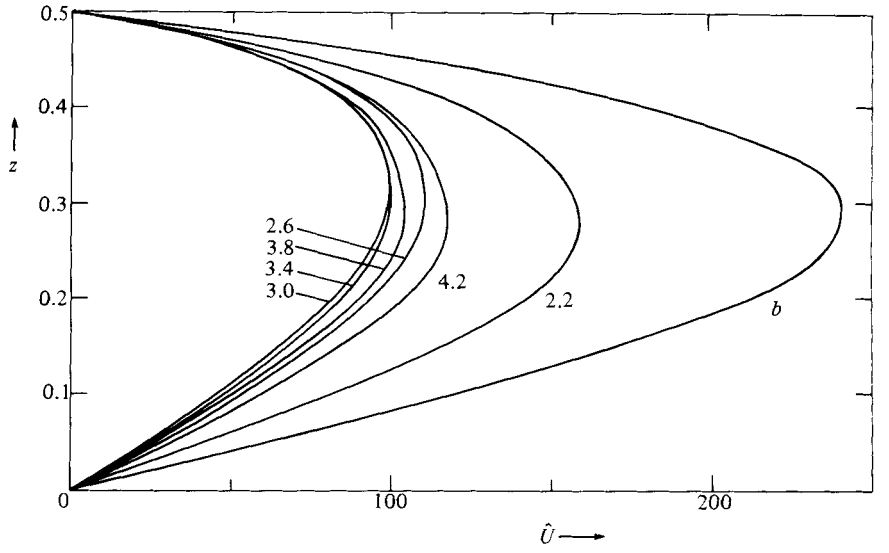

FIGURE 6. The mean flow $\hat{U}$ as a function of z for different wavenumbers at a fixed Grashof number $G = 30000$. The undisturbed flow $\hat{U} = U$ is indicated by b.

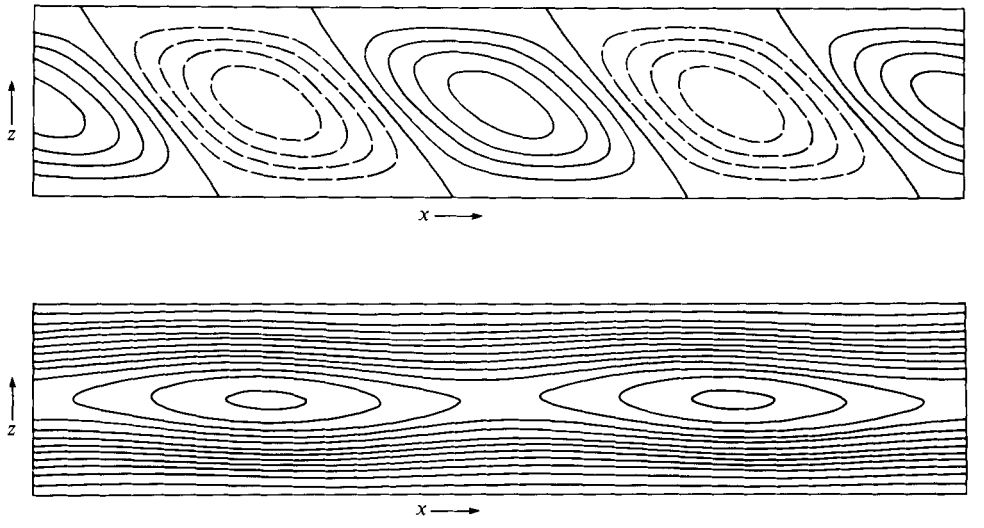

FIGURE 7. The stream function $\partial\phi/\partial x$ of the transverse vortices (upper part) and the streamfunction $\hat{U}z + \partial\phi/\partial x$ of the total flow (lower part) for $\alpha = 2.6$, $G = 9000$. Constant values of $\partial\phi/\partial x$ at increments of 20% of the maximum value are drawn in the upper part (negative contours are dashed). In the lower part the stream function is plotted with increments of 2.

4. Instabilities of transverse vortices

In order to investigate the stability of the steady transverse vortex solutions described in the preceding section we superimpose arbitrary three-dimensional infinitesimal disturbances and compute their growth rates. The steady solutions are unstable whenever growing disturbances are found. Since the equations for the disturbances are linear homogeneous and do not depend explicitly on y and t, an

exponential dependence on the latter two coordinates can be assumed. Describing the disturbance of the steady solution ϕ by $\tilde{\phi}$, $\tilde{\psi}$, we arrive at the general ansatz

$$\tilde{\phi} = \sum_{m=-\infty}^{\infty} \sum_{l=1}^{\infty} \tilde{a}_{lm} f_l(z) \exp\{\mathrm{i}m\alpha x + \mathrm{i}dx + \mathrm{i}by + \sigma t\}, \tag{4.1a}$$

$$\tilde{\psi} = \sum_{m=-\infty}^{\infty} \sum_{l=1}^{\infty} \tilde{b}_{lm} g_l(z) \exp\{\mathrm{i}m\alpha x + \mathrm{i}dx + \mathrm{i}by + \sigma t\}, \tag{4.1b}$$

where the functions $g_l(z)$ satisfying the boundary conditions for ψ are defined by

$$g_l(z) = \sin l\pi(z+\tfrac{1}{2}) \quad (l = 1, 2, \ldots). \tag{4.2}$$

In contrast with the representation (3.1a), the summation (4.1a) includes $m = 0$. Since the finite value of d^2+b^2 will be assumed throughout this section, there is no contribution to a perturbation of the mean flow $\hat{U}$. Disturbances with $d = b = 0$ are actually included in the analysis of the steady solution, even though the Newton–Raphson iteration models simulates only approximately the approach in time towards the steady solution. The boundary in figure 3 beyond which steady solutions could not be obtained, for example, is due to this instability; disturbances with twice the wavenumber replace the steady solution beyond that boundary. This boundary should not be called a stability boundary, however, since disturbances of the same character but with finite d grow more strongly than those with $d = 0$ and the appropriate stability boundary is thus given by the dashed line in figure 9.

The equations to be satisfied by $\tilde{\phi}$, $\tilde{\psi}$ are given by

$$\nabla^2\Delta_2\tilde{\phi} - \left\{\hat{U}\frac{\partial}{\partial x} + \sigma\right\}\nabla^2\Delta_2\tilde{\phi} + \frac{\mathrm{d}^2}{\mathrm{d}z^2}\hat{U}\frac{\partial}{\partial x}\Delta_2\tilde{\phi} - \boldsymbol{\delta}\cdot\{\boldsymbol{\delta}\tilde{\phi} + \boldsymbol{\epsilon}\tilde{\psi})\cdot\boldsymbol{\nabla}\boldsymbol{\delta}\phi + \boldsymbol{\delta}\phi\cdot\boldsymbol{\nabla}(\boldsymbol{\delta}\tilde{\phi} + \boldsymbol{\epsilon}\tilde{\psi})\} = 0, \tag{4.3a}$$

$$\nabla^2\Delta_2\tilde{\psi} - \left\{\hat{U}\frac{\partial}{\partial x} + \sigma\right\}\Delta_2\tilde{\psi} + \frac{\mathrm{d}}{\mathrm{d}z}\hat{U}\mathrm{i}b\Delta_2\tilde{\phi} - \boldsymbol{\epsilon}\cdot\{(\boldsymbol{\delta}\tilde{\phi} + \boldsymbol{\epsilon}\tilde{\psi})\,.\,\boldsymbol{\nabla}\boldsymbol{\delta}\phi + \boldsymbol{\delta}\phi\,.\,\boldsymbol{\nabla}(\boldsymbol{\delta}\tilde{\phi} + \boldsymbol{\epsilon}\tilde{\psi})\} = 0. \tag{4.3b}$$

After multiplying (4.3a) and (4.3b) by $f_\lambda(z)\exp\{-\mathrm{i}(\mu\alpha x + dx + by) - \sigma t\}$, and by $g_\lambda(z)\exp\{-\mathrm{i}(\mu\alpha x + dx + by) - \sigma t\}$ respectively, and averaging the result over the fluid layer, a system of linear homogeneous equations for the coefficients $\tilde{a}_{lm}$ and $\tilde{b}_{lm}$ is obtained with σ as eigenvalue. In order to evaluate the eigenvalues σ of interest, the infinite system of equations must be truncated. In general, the same truncation level (3.6a) was used as in the case of the steady solution. Since the eigenvalues σ of interest have nearly vanishing real part and either a zero or a relatively small imaginary part, they are not much affected by the truncation level if a well-approximated steady solution is used.

For a given steady solution characterized by the parameters G and α, the eigenvalue σ with maximum real part is determined as a function of b and d. Figure 8 indicates that there are typically two eigenvalues, a real one and two complex-conjugate ones whose real parts can reach positive values. In the limit of infinite truncation parameter N the results plotted in this figure are strictly periodic in d with period α. Because of the finite truncation, small deviations from periodicity are noticeable. By calculating the maximum real part at several Grashof numbers the value of G can be determined by interpolation at which the maximum real part of σ changes sign. This Grashof number as a function of α defines the stability boundary of the steady transverse vortices in the (G, α) parameter space. As shown in figure 9, this stability boundary is given by the monotonically growing disturbances. But,

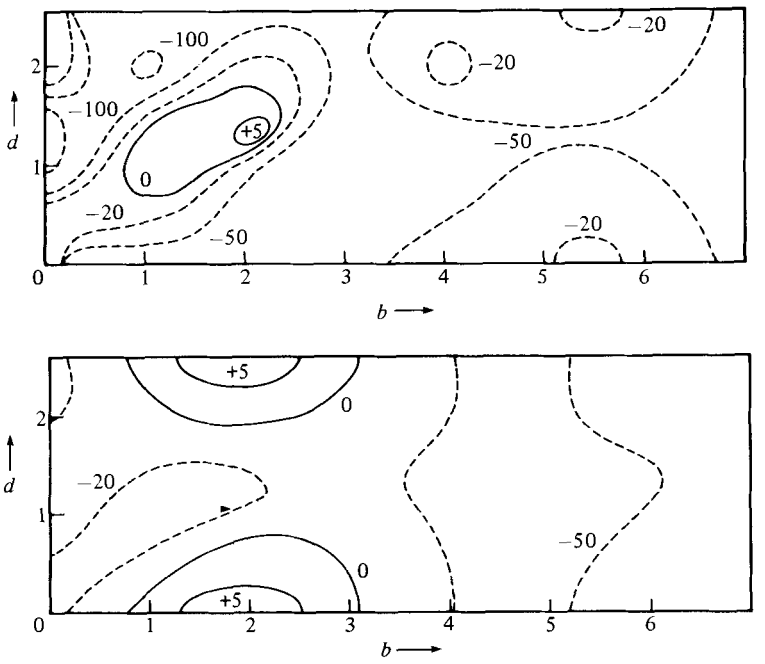

FIGURE 8. Real parts of σ as a function of b and d for $G = 10^4$, $\alpha = 2.6$. The upper part shows lines of constant growth rate (indicated by the numbers) for the monotone instability, the lower part shows the real part of σ for the oscillating instability.

since the oscillatory instability corresponding to the eigenvalue with finite imaginary part exhibits a maximum real part of nearly the same magnitude as the monotone instability, its stability boundary is also shown in figure 9. The value of b at the onset of the monotone instability changes little along the solid curve of figure 9 varying between 1.5 and 1.6, but the maximum growthrate always corresponds to $d = \frac{1}{2}\alpha$.

The Eckhaus instability which bounds the domain of the stable transverse vortices towards larger and lower wavenumbers derives its name from the first study of the stability of Tollmein–Schlichting waves (Eckhaus 1965). A flaw in this work was pointed out by Stuart & DiPrima (1978), who also demonstrated the equivalence between the Eckhaus instability and the sideband instability of Benjamin & Feir (1967). The Eckhaus or sideband instability is characterized by $b = 0$ and thus does not depend on the third dimension. The growth rate σ as a function of d is shown in figure 10 for some typical wavenumbers. A characteristic property is the minimum of σ at $d = \frac{1}{2}\alpha$, which indicates that an instability introducing vortices with twice the wavelength of the original vortices is not preferred. This result differs considerably from the conclusions of Kelly (1967) and Pierrehumbert & Widnall (1982) based on inviscid analysis. These authors considered only the case $d = \frac{1}{2}\alpha$ and found an instability owing to the growth of subharmonic vortices. No indication of such an instability was found in the present analysis since the Eckhaus instability only limits the wavenumber domain of stable vortices, but does not cause a transition as the Grashof number is increased at a fixed value of α.

Since the flow generated by the monotone instability will be discussed in §5, we briefly describe here the spatial structure of growing oscillatory disturbances. Figure 11 shows the wavy structure which develops if a growing disturbance multiplied by an arbitrary amplitude factor is superimposed onto the steady

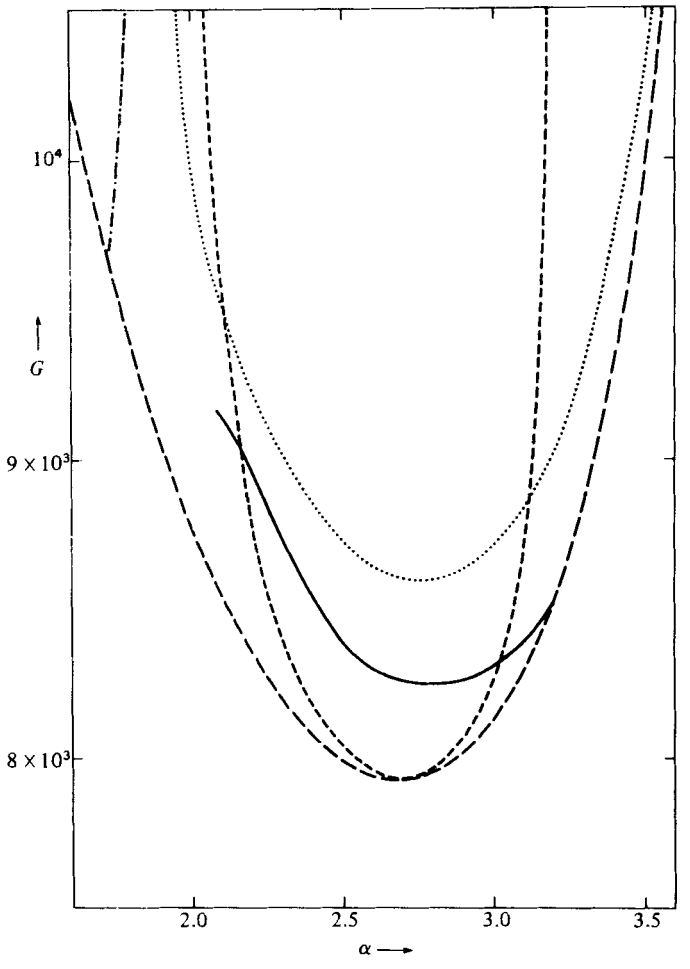

FIGURE 9. Stability regime of transverse vortices. The outer parabolic curve (long dashes) indicates results of linear theory. The region of stable vortices is bounded by the Eckhaus stability boundary (short dashes) from below and the monotone instability (solid line) from above. The boundary of onset of oscillatory instability (dotted line) is also shown. Steady solutions could not be obtained in the region left of the dash-dotted line.

transverse vortices. The waves propagate in the positive or negative y-directions. Standing waves correspond to the superposition with equal amplitude of both propagating waves are also a plausible possibility. Associated with the oscillation is the generation of vertical vorticity described by the function $\tilde{\psi}$, which is shown in figure 12. The vertical vorticity is mainly caused by the advection of the mean momentum by the poloidal component of the disturbance described by $\tilde{\phi}$.

The oscillatory instability corresponds to $d = 0$, in which case disturbances of the form (4.1) separate in two classes of different symmetry. The determinant determining the eigenvalue σ becomes the product of two determinants corresponding to

$$\text{class A:} \quad \tilde{a}_{lm} = \pm \tilde{a}^*_{lm} \quad \left(l+m \begin{Bmatrix} \text{even} \\ \text{odd} \end{Bmatrix}\right); \tag{4.4a}$$

$$\text{class B:} \quad \tilde{a}_{lm} = \mp \tilde{a}^*_{lm} \quad \left(l+m \begin{Bmatrix} \text{even} \\ \text{odd} \end{Bmatrix}\right). \tag{4.4b}$$

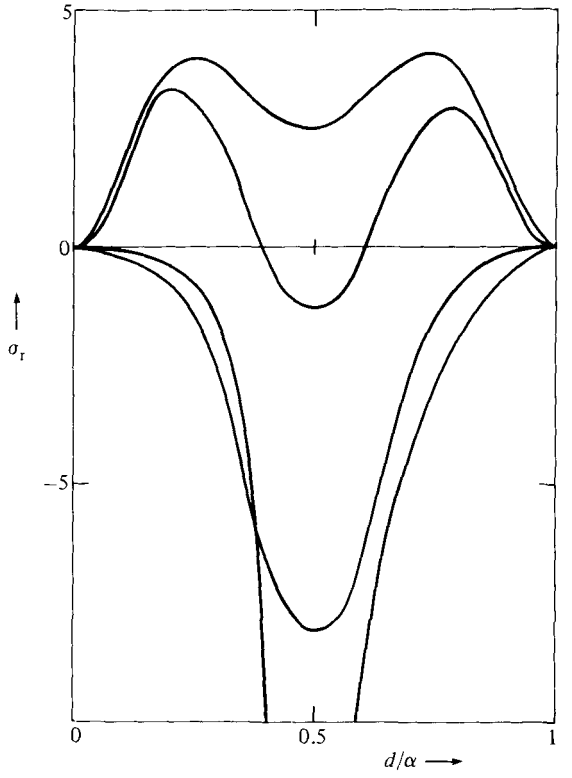

FIGURE 10. The growth rate of the Eckhaus instability as a function of d for several wavenumbers α at $G = 9000$.

Disturbances of class A exhibit the same symmetry (3.5) as the steady transverse vortices and do not give rise to instability in range of G studied in this paper. A special disturbance of class B corresponding to $\sigma = 0$ is given by $\phi = \partial\phi/\partial x$ and describes an infinitesimal translation of the steady vortex solution. As in the case of convection, the oscillatory instability represents a modification of the translational disturbance (Busse 1972). The details of the dependence of the eigenvalue σ on b are complicated by the fact that the imaginary part vanishes for sufficiently small values of b as shown in figure 13. The eigenvalue starting with $\sigma = 0$ at $b = 0$ joins with another real eigenvalue σ as b increases, at which point the two eigenvalues separate into two complex-conjugate eigenvalues. For low values of G the same process occurs in reverse order as b exceeds a second critical value. For supercritical Grashof numbers the real part of the complex eigenvalue reaches a maximum around $b = 2.0$. The value of b that maximizes the growth rate changes little as a function of α, and the dotted curve in figure 9 has therefore been obtained by calculating the Grashof number at which the real part of σ changes sign for $b = 2.0$.

This oscillatory instability is closely related to the oscillatory instability discussed by Pierrehumbert & Widnall (1982), although some of the properties are quite different. In their case two imaginary eigenvalues σ join as b increases and are transformed into two complex-conjugate eigenvalues. Because of the absence of dissipation there is no clear maximum at which the growth rate peaks, while in the present case a preferred wavenumber $b \approx 2$ is clearly discernible. But in their spatial dependence the two forms of oscillatory instability resemble each other closely.

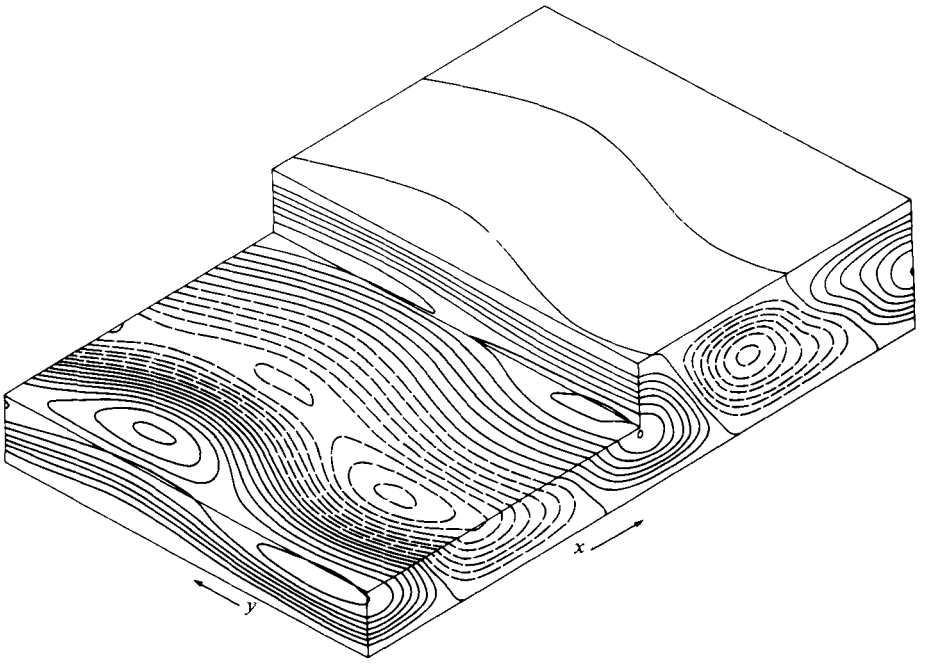

FIGURE 11. Lines of constant vertical velocity $u_z \equiv -\Delta_2\phi - \epsilon\Delta_2\tilde{\phi}$ in the case of oscillatory instability for $G = 9000$, $\alpha = 2.6$, $b = 2.0$. The factor ϵ denotes the amplitude of the oscillatory disturbance and has been fixed at some small, but otherwise arbitrary, value. Negative values of u_z are indicated by dashed lines.

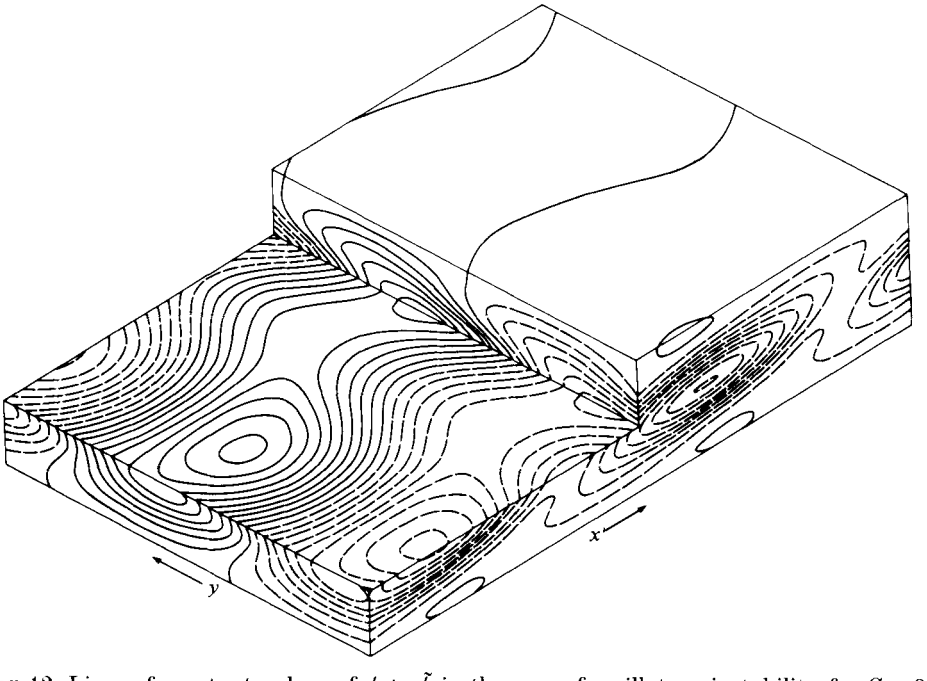

FIGURE 12. Lines of constant values of $\psi + \epsilon\tilde{\psi}$ in the case of oscillatory instability for $G = 9000$, $\alpha = 2.6$, $b = 2.0$. The value of ϵ is the same as in figure 11. Negative values of ψ are indicated by dashed lines.

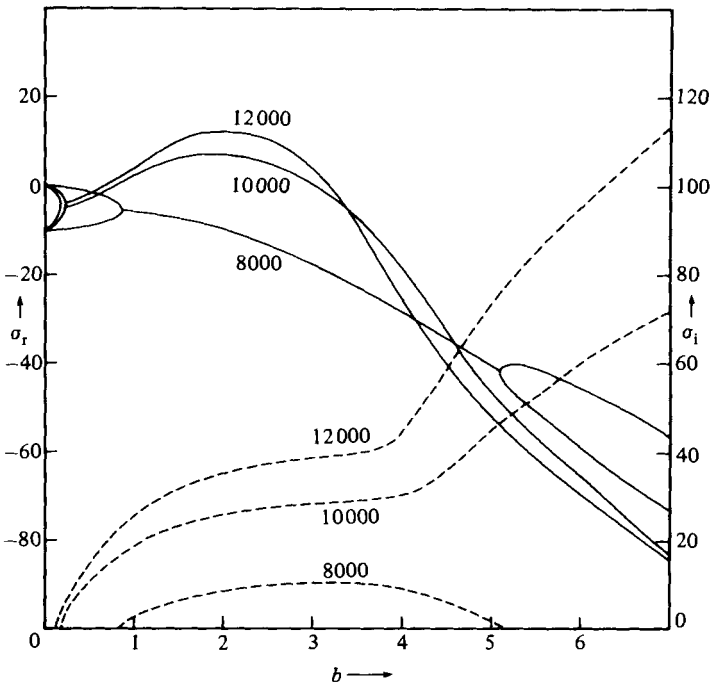

FIGURE 13. Real (solid lines, left ordinate) and imaginary (dashed lines, right ordinate) parts of σ for the oscillatory instability as a function of the spanwise wavenumber b for selected values of G as indicated by the numbers in the figure. The streamwise wavenumber α is 2.6 in all cases.

5. Steady three-dimensional flow

The finding that two-dimensional vortex flow becomes unstable to three-dimensional disturbances relatively soon after the Grashof number exceeds its critical value has stimulated the attempt to study three-dimensional solutions of the basic equations (2.7). Obviously the cost of computing is increased considerably in this step from two to three dimensions, and only a rather restricted exploration of the tertiary flow and its instabilities could be accomplished.

Since the monotone instability limits the region of stable secondary flow in the form of transverse vortices, only steady three-dimensional solutions have been investigated. The maximum growth rate of the monotone instability as a function of the wavenumbers b and d motivates the choice of parameters. In particular, because of the wavelength-doubling property of the instability, a wavenumber α equal to one half of the corresponding wavenumber of transverse vortices is chosen. Accordingly the following representation for ϕ and ψ is assumed:

$$\phi = \sum_{l,m,n} a_{lmn} \exp\{\mathrm{i}(m\alpha x + n\beta y)\} f_l(z), \tag{5.1a}$$

$$\psi = \sum_{l,m,n} b_{lmn} \exp\{\mathrm{i}(m\alpha x + n\beta y)\} g_l(z). \tag{5.1b}$$

where l runs through positive integers only, while m and n run through both positive and negative integers excluding the case $m = n = 0$. Without losing generality it can be assumed that ϕ is a symmetric function of y. The symmetry of (2.7) then requires that ψ is antisymmetric in y:

$$a_{lm-n} = a_{lmn}, \quad b_{lm-n} = -b_{lmn}. \tag{5.2}$$

Because (5.1) are real, the complex conjugate of the coefficients a_{lmn}, b_{lmn} is obtained when both subscripts m, n change sign. There are further symmetry properties which can be used to restrict the number of unknowns. Because the solution of the form (5.1) bifurcates from a y-independent solution with vanishing coefficients for odd values of m, the symmetry properties

$$a_{lmn} = b_{lmn} = 0 \quad (m+n \text{ odd}), \tag{5.3a}$$

$$a_{lmn} = \pm a^*_{lmn} \quad \left(l+m\begin{Bmatrix}\text{even}\\ \text{odd}\end{Bmatrix}\right), \tag{5.3b}$$

$$b_{lmn} = \mp b^*_{lmn} \quad \left(l+m\begin{Bmatrix}\text{odd}\\ \text{even}\end{Bmatrix}\right) \tag{5.3c}$$

are obtained. These properties do not include the property (3.5) of the two-dimensional solution (3.1a). But, if that solution is shifted by half a wavelength in the x-direction, then

$$a_{lm} = \pm a^*_{lm} \quad \left(l\begin{Bmatrix}\text{even}\\ \text{odd}\end{Bmatrix}\right) \tag{5.4}$$

is obtained instead of (3.5), in agreement with property (5.3b) if it is remembered that (5.4) applies to those coefficients a_{lmn} for which n vanishes and m is an even integer. In addition to the representations (5.1), the description (3.1b) for the mean flow must be included in the analysis of the problem.

After introducing (5.1), (3.1b) into (2.7), (2.8), and after multiplying the equations by the complex conjugates of the expansion functions and averaging them, nonlinear algebraic equations are obtained for the coefficients a_{lmn}, b_{lmn} and C_k. For the numerical solution, coefficients and equations with subscripts satisfying

$$2l+|m|+2|n| > N_1^*, \quad k > N_2^* \tag{5.5a, b}$$

have been dropped in analogy to the truncation (3.6). The truncation (5.5a) takes into account the fact that the transverse-vortex solution from which the presently considered three-dimensional solution bifurcates corresponds to even subscripts m. Typical values of the truncation parameter are $N_1^* = 14$, $N_2^* = 6$, which appear to provide an adequate approximation of the three-dimensional solution. Since this truncation leads to a total of 102 unknowns, the approximation could not be tested as extensively as in the two-dimensional case. Although not as many higher harmonics in the x- or z-directions are taken into account, the convergence appears to be faster because of the additional degree of freedom available in the three-dimensional solution for the dissipation of energy.

Solutions of the form (5.1) have been obtained for selected values of G, α and β. Since the monotone instability does not depend strongly on α, the latter parameter has been fixed at $\alpha = 1.3$ for the majority of computations. There exists a finite range of wavenumbers β for which three-dimensional solutions could be obtained. Although the critical wavenumber β is 1.6 for $\alpha = 1.3$ (corresponding to $\alpha = 2.6$ of the transverse vortices), $\beta = 2.0$ appears to be preferred at higher Grashof numbers, as indicated by maximum growth rate on figure 8. The three-dimensional flow appears to evolve smoothly from the transverse-vortex solution as G increases beyond the stability boundary of figure 9. There is no indication of subcritical finite-amplitude three-dimensional flow. The distortion of the transverse vortices by the three-dimensional effects is shown in figure 14. The corresponding pattern of the function ψ is displayed in figure 15. As the disturbance of the two-dimensional structure grows to large amplitudes at the higher values of G, the pairing of neighbouring vortices

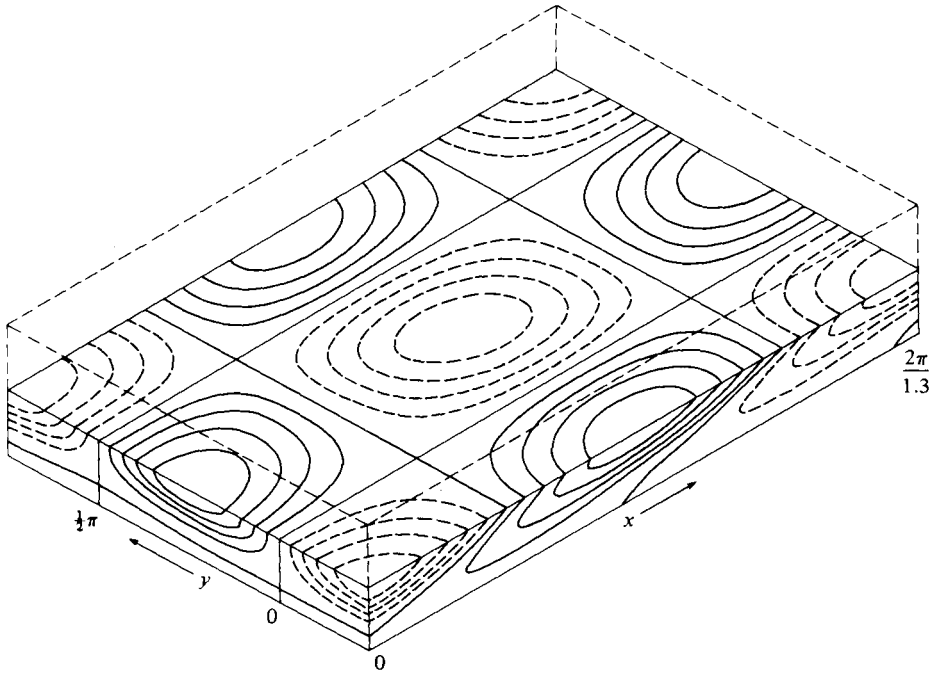

FIGURE 14. Lines of constant vertical velocity $u_z = -\Delta_2 \phi$ in the plane $z = 0$ for $G = 9000$, $\alpha = 1.3$, $\beta = 2.0$. Lines corresponding to negative values are dashed.

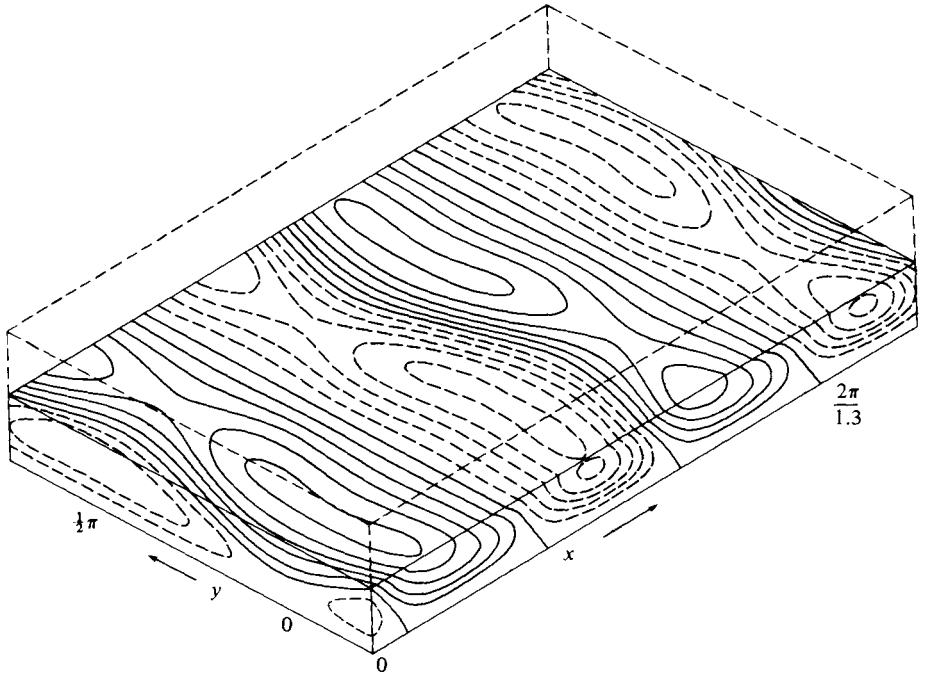

FIGURE 15. Lines of constant ψ in the plane $z = 0$ for $G = 9000$, $\alpha = 1.3$, $\beta = 2.0$.

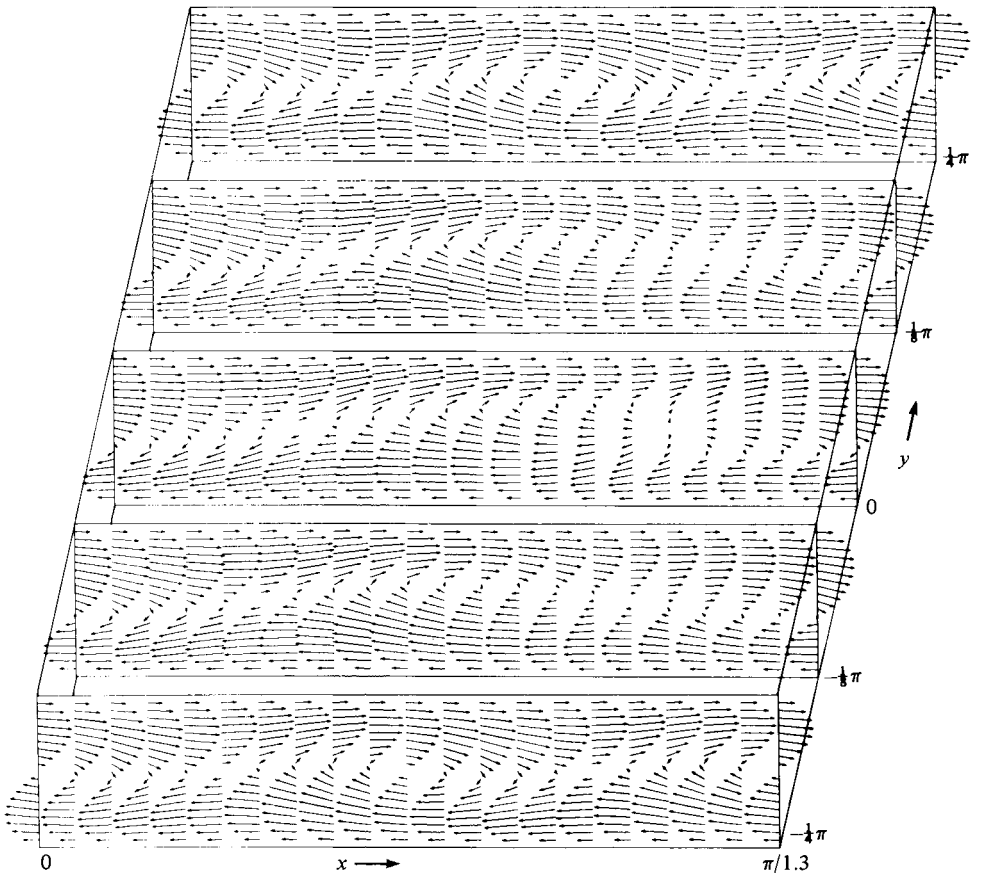

FIGURE 16. Velocity vectors in the planes $y = n\pi/4\beta$, $n = -2, -1, 0, 1, 2$, for $G = 12000$, $\alpha = 1.3$, $\beta = 2.0$.

becomes apparent, alternating in the forward and backward directions. Figure 16 indicates that the 'cat's-eyes' shift forward and backward in a periodic manner along the spanwise coordinate and join with the neighbouring 'cat's-eyes' in the streamwise direction. Because of the slight tilt of the transverse vortices, the forward-moving sections of these vortices tend to be elevated while the backward-moving parts tend to descend. The x, y-components of vorticity shown in the plane $z = 0$ (figure 17) indicate clearly the alternating pairing of vortices. In this respect the present results support the interpretation of the corresponding instability in the inviscid analysis of Pierrehumbert & Widnall (1982, see their figure 6). It should be noted, however, that the 'cat's-eyes' do not necessarily indicate a local maximum of vorticity. Stretching and compression of vortex tubes have a strong effect on the magnitude of the vorticity vector, as is evident when figure 17 is considered in conjunction with figure 18, which exhibits the spanwise component of the velocity field.

A different interpretation of three-dimensional solution is based on the triad interaction of the three planar waves in the (x, y)-plane with wavevectors $(\pm 2\alpha, 0)$, $(\mp\alpha, \beta)$, $(\mp\alpha, -\beta)$. A resonant-triad interaction was proposed by Craik (1971) as the dominant nonlinear process in the instability of plane boundary layers. In the present case no resonance is required because of the symmetry of the problem. In contrast

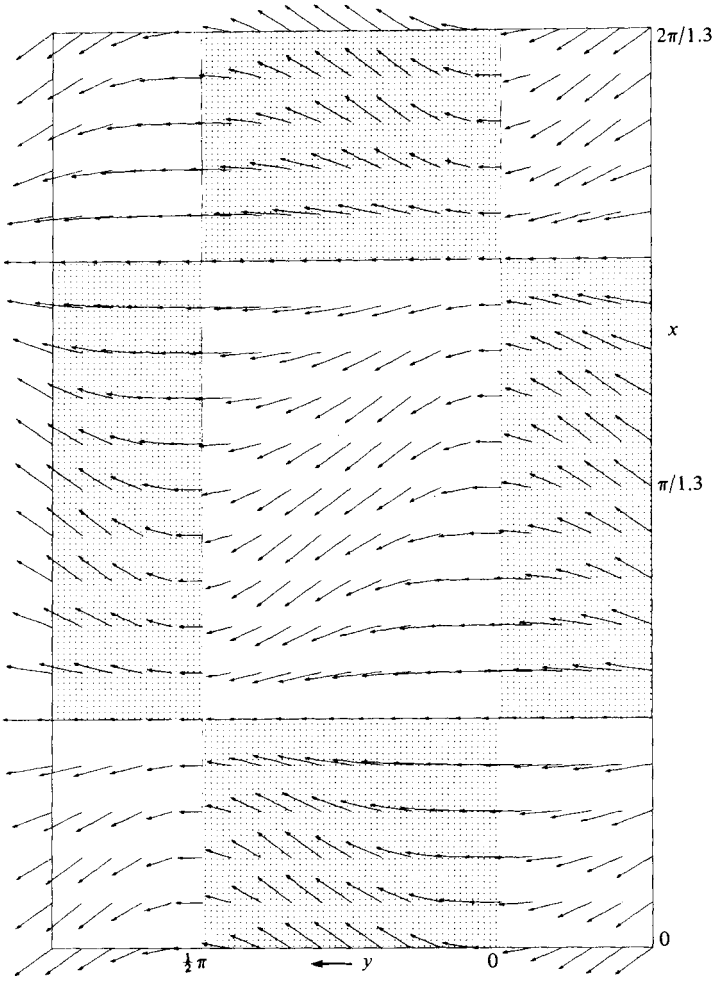

FIGURE 17. The horizontal component of the vorticity vector in the plane $z = 0$. Shaded areas indicate a positive value of the vertical component of the vorticity vector. The arrows show the bending of vortex tubes in the forward and backward direction indicating the pairing of the transverse vortices. See figure 16 for comparison.

to the scenario proposed by Craik the triad interaction is actually less effective in transferring energy from the mean flow into fluctuating motion than the transverse vortices. This is apparent in figure 19, where the energies of the different components of motion have been plotted. The main transfer of energy is from the transverse component of the vortices into the longitudinal components, while the total energy of the fluctuating motion is nearly the same as for the two-dimensional solution.

As suggested by figure 19, the amplitude of the mean flow is larger for the three-dimensional solution than for the two-dimensional solution at the same Grashof number, but the positions of the extrema in the profile $\hat{U}(z)$ remain unchanged. Only the shear $\mathrm{d}\hat{U}/\mathrm{d}z$ at the median plane of the layer is slightly less in the three-dimensional case, in accordance with the property that the curvature of the profile $\hat{U}(z)$ near the median plane is decreased. The instability of the transverse vortices thus leads to a

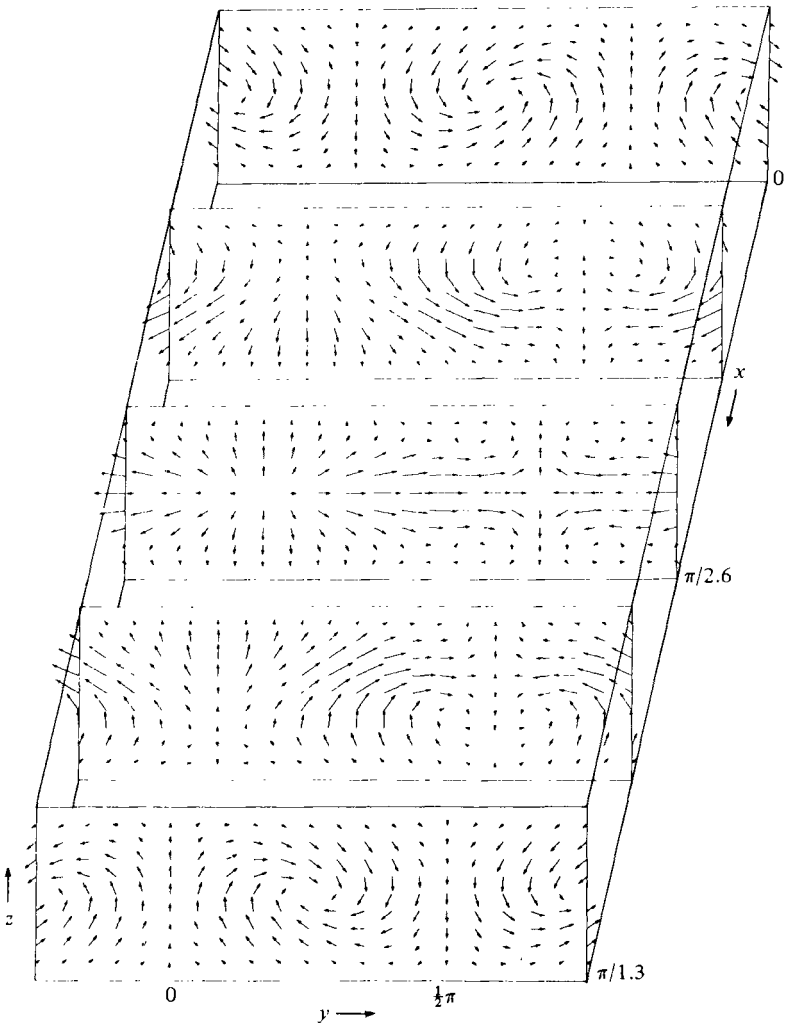

FIGURE 18. The y- and z-components of the velocity vector in the planes $x = n\pi/4\alpha$, $n = 0, 1, 2, 3, 4$.

three-dimensional flow whose momentum transport is slightly more effective near the middle of the layer, but which overall is significantly less effective than the two-dimensional flow.

6. Instabilities of steady three-dimensional flow

The fact that monotone and oscillatory instabilities of transverse vortices are occurring in close competition according to figures 8 and 9 suggests that the three-dimensional flow discussed in §5 may not be very stable. Indeed, as will become apparent in the following, the oscillatory instability is only slightly suppressed by the growth of three-dimensional structure. It reappears in a modified form at higher Grashof numbers and ultimately leads to the destruction of the three-dimensional steady flow.

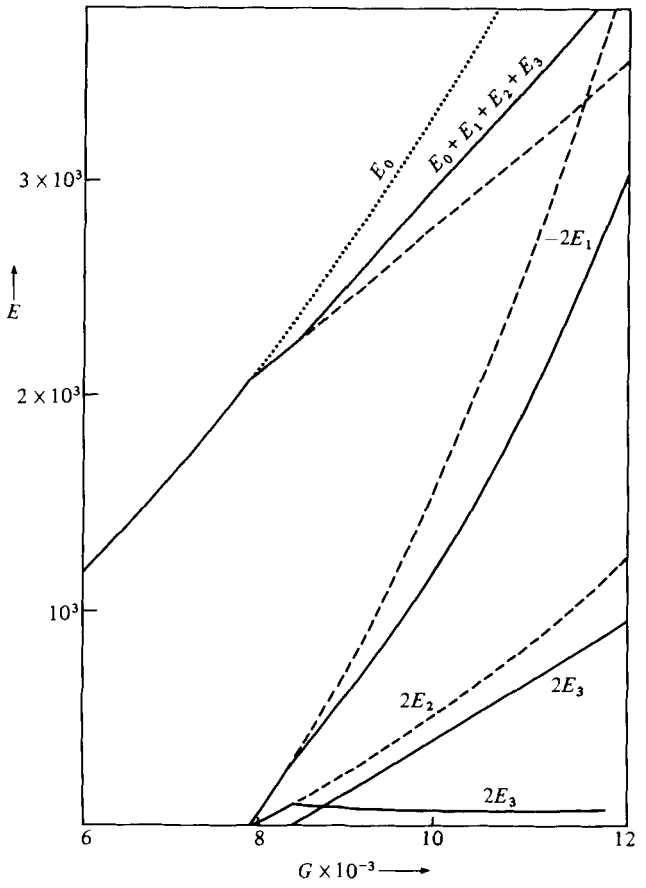

FIGURE 19. Average kinetic energies of primary, secondary, and tertiary steady flows. The definitions

$$E_0 = \langle U^2 \rangle, \quad E_1 = \langle \tilde{U}^2 \rangle - E_0, \quad E_2 = \langle |\phi \nabla^2 \Delta_2 \phi|_{n=0} \rangle \quad \text{with} \quad \alpha = 2.6,$$
$$E_3 = \langle |\phi \nabla^2 \Delta_2 \phi|_{n\neq 0} + |\psi \Delta_2 \psi| \rangle \quad \text{with} \quad \alpha = 1.3, \quad \beta = 2.0$$

have been used, where the subscript n refers to the spanwise wavenumber included in the funtion ϕ. E_2 thus describes the kinetic energy of the fluctuating component of motion which does not depend on y, while E_3 describes the kinetic energy of the velocity component with zero mean in the y-direction.

The primary solution of the basic equations is indicated by a solid line for $G < 7930$ and by a dotted line for $G \geqslant 7930$. The second solution is given by the solid line for $7930 < G \leqslant 8400$ and by a dashed line thereafter. For $G \geqslant 8400$ the solid line describes the tertiary solution.

In analysing disturbances of the steady three-dimensional flow we are particularly concerned with instabilities introducing new wavenumbers in the y-direction. In order to reduce the complexity of the instability analysis we therefore neglect the Floquet exponent for the x-dependence and assume as representation for the disturbances

$$\tilde{\phi} = \sum_{l,m,n} \tilde{a}_{lmn} \exp\{\mathrm{i}(m\alpha x + n\beta y) + \mathrm{i}by + \sigma t\} f_l(z), \tag{6.1a}$$

$$\tilde{\psi} = \sum_{l,m,n} \tilde{b}_{lmn} \exp\{\mathrm{i}(m\alpha x + n\beta y) + \mathrm{i}by + \sigma t\} g_l(z). \tag{6.1b}$$

Because of the symmetry properties (5.2), (5.3) of the steady three-dimensional

solution, the stability equations for disturbances of the form (6.1) permit the following classes of solutions:

$$\text{class A:}\quad \tilde{a}_{lmn} = 0 \quad (m+n \text{ odd}), \tag{6.2a}$$

$$\tilde{a}_{lmn} = \pm a^*_{lmn} \quad \left(l+m\begin{Bmatrix}\text{even}\\ \text{odd}\end{Bmatrix}\right); \tag{6.2b}$$

$$\text{class B:}\quad \tilde{a}_{lmn} = 0 \quad (m+n \text{ odd}), \tag{6.3a}$$

$$\tilde{a}_{lmn} = \pm \tilde{a}^*_{lmn} \quad \left(l+m\begin{Bmatrix}\text{even}\\ \text{odd}\end{Bmatrix}\right). \tag{6.3b}$$

In addition there are two classes differing from classes (6.2), (6.3) only in that $\tilde{a}_{lmn}$ vanishes for even $m+n$ instead of odd $m+n$. But these latter classes are represented by (6.2), (6.3) if b is replaced by $b \pm \beta$. They thus require no separate considerations.

The two classes of disturbances (6.2) and (6.3) can be characterized to some extent by two special disturbances given by

$$\tilde{\phi} = \frac{\partial}{\partial y}\phi, \quad \tilde{\psi} = \frac{\partial}{\partial y}\psi \quad \text{in the case of class A;} \tag{6.4}$$

$$\tilde{\phi} = \frac{\partial}{\partial x}\phi, \quad \tilde{\psi} = \frac{\partial}{\partial x}\psi \quad \text{in the case of class B.} \tag{6.5}$$

These disturbances correspond to infinitesimal translations of the steady solution in the y- and x-directions respectively, and thus solve the stability equations for $b = \sigma = 0$. For finite values of b the disturbances of classes A and B do not exhibit a particular symmetry with respect to the y-direction, but with respect to the x-direction disturbances of class B tend to shift the phase of the steady solution, in contrast with those of class A.

Computations of the eigenvalues σ with largest real part as a function of b indicate that the most strongly growing disturbances belong to class B. In particular, a disturbance with finite imaginary part σ_i attains a maximum real part for $b = 1 + n\beta$, $n = 0, \pm 2, \ldots$, which becomes positive when G exceeds the critical value $G^{(0)} = 11060$. Because of the symmetry property (6.3a) σ must be a periodic function of b with period 2β in the limit of infinite truncation parameter. As discussed in §4, this periodicity is only approximately realized in the case of a finite truncation N^*. The oscillatory instability represents a period-doubling subharmonic disturbance with respect to the spanwise dependence of the steady three-dimensional flow. The structure of the latter is shifted backward and forward periodically in time and with a wavelength twice that of the steady flow in the spanwise direction. The fact that the wavelength in the spanwise direction is also twice as big as that of the oscillatory instability of transverse vortices exhibited in figure 8(b) is not surprising, since the streamwise wavelength has doubled in the transition from two-dimensional to three-dimensional flow. The frequency of oscillation is ± 4.6 at $G = G^{(0)}$, which is relatively small in comparison with the values shown in figure 13. Part of this decrease can be attributed to the larger wavelength of the steady flow in the streamwise direction. The remaining discrepancy may be caused by the weakened transverse vortex component of the three-dimensional flow.

Because of the high costs of computations of the eigenvalues – the rank of the stability matrices is typically 214 – only a limited number of cases have been explored, and our conclusions depend on a smooth dependence of the eigenvalues σ

on the parameters of the problem. The parameters α and β of the steady solution were usually restricted to the values 1.3 and 2.0 respectively, although some computations have been carried out with $\beta = 2.5$ at higher values of the Grashof number. More detailed computations would be warranted if contact with the experimental evidence could be made. But little appears to be known either from the experiments of Thomas & Saric (1981) or others about the nature of the breakdown of the three-dimensional staggered structures which most closely appear to resemble the three-dimensional steady solution studied in this paper.

7. Discussion

The symmetry with respect to the median plane of the layer in the problem considered in this paper is responsible for the particularly simple transitions to three-dimensional forms of motion that have been analysed in the preceding sections. Even in the transition to the tertiary mode of flow, no time dependence is introduced, and the complexities of interacting waves propagating with different phase velocities are avoided. It is desirable to study the problem experimentally, since the available laboratory data do not provide information about three-dimensional aspects of the motion.

There are a variety of mechanisms of transition to three-dimensional flow in shear layers that have been discussed in the literature. The experimental evidence indicates that slight changes in the shear-flow profile or in the level of noise present in the experimental apparatus may lead to qualitatively different transitions (see e.g. Thomas & Saric 1981). The close competition between different mechanisms of instability such as the monotone and oscillatory instability discussed in §4 is likely to be responsible for this experimental phenomenon. While the physical effects that may lead to the predominance of one or the other mechanism of instability could not be studied in this paper, some general properties can be recognized. The comparison of the present analysis with that of Kelly (1967) and Pierrehumbert & Widnall (1982) suggests that in the absence of boundaries the two-dimensional wavelength-doubling instability is preferred, in contrast with the three-dimensional subharmonic instability of the present analysis. This finding agrees with the observed two-dimensional vortex pairing in mixing layers (Brown & Roshko 1974), while a staggered pattern like the one shown in figure 17 is observed in the breakdown of two-dimensional Tollmien–Schlichting waves in boundary layers (Thomas & Saric 1981). The importance of the boundaries in favouring the three-dimensional subharmonic instability investigated in this paper is also supported by the analysis of Herbert (1983) of the instability of Tollmien–Schlichting waves in plane Poiseuille flow.

There is another instability introducing three-dimensional structure in transverse vortices without changing the phase of those vortices. This instability is characterized by a value of b of the same order or larger than the wavenumber α of the transverse vortices. It appears to give rise to longitudinal vortices of alternating sign (Breidenthal 1982). The fact that this instability was not found in the present analysis, at least not at Grashof numbers up to the order of 15000, suggest that it is also inhibited by the presence of boundaries.

The research reported in this paper has been supported by the Atmospheric Science Section of U.S. National Science Foundation. Preliminary results of the study have been reported at the Fluid Dynamics Meeting of the American Physical Society at Monterey, November 1981 (Nagata & Busse 1981).

REFERENCES

BENJAMIN, T. B. & FEIR, J. E. 1967 The disintegration of wave trains on deep water. Part 1. Theory. *J. Fluid Mech.* **27**, 417–430.

BENNEY, D. J. & BERGERON, R. F. 1969 A new class of nonlinear waves in parallel flows. *Stud. Appl. Maths* **48**, 181–204.

BREIDENTHAL, R. 1981 Structure in turbulent mixing layers and wakes using a chemical reaction. *J. Fluid Mech.* **109**, 1–24.

BROWN, G. L. & ROSHKO, A. 1974 On density effects and large structure in turbulent mixing layers. *J. Fluid Mech.* **64**, 775–816.

BUSSE, F. H. 1967 On the stability of two-dimensional convection in a layer heated from below. *J. Maths & Phys.* **46**, 140–150.

BUSSE, F. H. 1972 The oscillatory instability of convection rolls in a low Prandtl number fluid. *J. Fluid Mech.* **52**, 97–112.

BUSSE, F. H. 1981 Transition to turbulence in Rayleigh–Bénard convection. In *Hydrodynamic Instabilities and the Transition to Turbulence* (ed. H. L. Swinney & J. P. Gollub), pp. 97–137. Springer.

CHANDRASEKHAR, S. 1961 *Hydrodynamic and Hydromagnetic Stability.* Oxford University Press.

CLEVER, R. M. & BUSSE, F. H. 1974 Transition to time-dependent convection. *J. Fluid Mech.* **65**, 625–645.

CRAIK, A. D. D. 1971 Non-linear resonant instability in boundary layers. *J. Fluid Mech.* **50**, 393–413.

DIPRIMA, R. C. & SWINNEY, H. L. 1981 Instabilities and transition in flow between concentric rotating cylinders. In *Hydrodynamic Instabilities and the Transition to Turbulence* (ed. H. L. Swinney & J. P. Gollub), pp. 139–180. Springer.

ECKHAUS, W. 1965 *Studies in Non-Linear Stability Theory.* Springer.

HABERMAN, R. 1972 Critical layers in parallel flows. *Stud. Appl. Maths* **51**, 139–161.

HELMHOLTZ, H. VON 1868 On discontinuous movements of fluids (transl. from the German by F. Guthrie) (4) **36**, 337–346.

HERBERT, T. 1981*a* A secondary instability mechanism in plane Poiseuille flow. *Bull. Am. Phys. Soc.* **26**, 1257.

HERBERT, T. 1981*b* Stability of plane Poiseuille flow: theory and experiment. *Rep.* VPI-E-81-35. *Virginia Polytechnic Institute and State University Blacksburg, Va.* 24061.

HERBERT, T. 1983 Secondary instability of plane channel flow to subharmonic three-dimensional disturbances. *Phys. Fluids* **26**, 871–874.

HUERRE, P. 1980 The nonlinear stability of a free shear layer in the viscous critical layer regime. *Phil. Trans. R. Soc. Lond.* **A293**, 643–675.

HUERRE, P. & SCOTT, J. F. 1980 The effect of critical layer structure on the nonlinear evolution of waves in free shear layers. *Proc. R. Soc. Lond.* **A371**, 509–324.

KELLY, R. E. 1967 On the stability of an inviscid shear layer which is periodic in space and time. *J. Fluid Mech.* **27**, 657–689.

KELVIN, LORD 1871 Hydrokinetic solutions and observations. *Phil. Mag.* (4), **42**, 362–377.

KORPELA, S. A., GÖZÜM, D. & BAXI, C. B. 1973 On the stability of the conduction regime of natural convection in a vertical slot. *Intl J. Heat Mass Transfer* **16**, 1683–1690.

NAGATA, M. 1983 Bifurcations in nonlinear problems of hydrodynamic instability of plane parallel shear flows. Ph.D. thesis, University of California, Los Angeles.

NAGATA, M. & BUSSE, F. H. 1981 Secondary motions in a simple plane parallel shear flow. *Bull. Am. Phys. Soc.* **26**, 1257.

ORSZAG, S. A. & KELLS, L. C. 1980 Transition to turbulence in plane Poiseuille and plane Couette flow. *J. Fluid Mech.* **96**, 159–205.

ORSZAG, S. A. & PATERA, A. T. 1980 Subcritical transition to turbulence in plane channel flows. *Phys. Rev. Lett.* **45**, 989–992.

PIERREHUMBERT, R. T. & WIDNALL, S. E. 1982 The two- and three-dimensional instabilities of a spatially periodic shear layer. *J. Fluid Mech.* **114**, 59–82.

RAYLEIGH, LORD 1880 On the stability, or instability, of certain fluid motions. *Proc. Lond. Math. Soc.* **11**, 57–70.

RUDAKOV, R. N. 1967 Spectrum of perturbations and stability of convective motion between vertical plates. *Prikl. Mat. Mekh.* **31**, 349–355.

RUTH, D. W. 1979 On the transition to transverse rolls in an infinite vertical fluid layer – a power series solution. *Intl J. Heat Mass Transfer* **22**, 1199–1208.

SCHADE, H. 1964 Contribution to the nonlinear stability theory of inviscid shear layers. *Phys. Fluids* **7**, 623–628.

SQUIRE, H. B. 1933 On the stability for three-dimensional disturbances of viscous fluid flow between parallel walls. *Proc. R. Soc. Lond.* **A142**, 621–628.

STUART, J. T. 1967 On finite amplitude oscillations in laminar mixing layers. *J. Fluid Mech.* **29**, 417–440.

STUART, J. T. & DIPRIMA, R. C. 1978 The Eckhaus and Benjamin–Feir Resonance Mechanism. *Proc. R. Soc. Lond.* **A362,** 27–41.

THOMAS, A. S. W. & SARIC, W. S. 1981 Harmonic and subharmonic waves during boundary layer transition. *Bull. Am. Phys. Soc.* **26**, 1252.

VEST, C. M. & ARPACI, V. S. 1969 Stability of natural convection in a vertical slot. *J. Fluid Mech.* **36**, 1–15.